Valley relaxation in a single-electron bilayer graphene quantum dot

Lin Wang and Guido Burkard
Department of Physics, University of Konstanz, D-78457 Konstanz, Germany

(Received 28 February 2024; accepted 14 June 2024; published 8 July 2024)

We investigate the valley relaxation due to intervalley coupling in a single-electron bilayer graphene quantum dot. The valley relaxation is assisted by both the emission of acoustic phonons via the deformation potential and bond-length change mechanisms and $1/f$ charge noise. In the perpendicular magnetic-field dependence of the valley relaxation time T_1, we predict a monotonic decrease of T_1 at higher fields due to electron-phonon coupling, which is in good agreement with recent experiments by Banszerus *et al.* (arXiv:2402.16691). We find that the dominant valley relaxation channel in the high-field regime is the electron-phonon coupling via the deformation potential. At lower fields, we predict that a peak in T_1 can arise from the competition between $1/f$ charge noise and electron-phonon scattering due to bond-length change. We also find that the interlayer hopping γ_3 opens a valley relaxation channel for electric charge noise for rotationally symmetric quantum dots in bilayer graphene.

DOI: 10.1103/PhysRevB.110.035409

I. INTRODUCTION

Bernal-stacked bilayer graphene (BLG) has a tunable band gap controlled by an out-of-plane electric field [1–7]. This semiconducting property enables the formation of quantum dots (QDs) in BLG via electrostatically induced quantum confinement. The possibility of hosting electron spin qubits in graphene-based QDs [8] has received some attention due to their expected long-lasting spin coherence including low hyperfine interaction and weak spin-orbit coupling [9–18]. Recently, long spin relaxation times of a single-electron state in BLG QDs exceeding 200 μs [19] and even up to 50 ms [20] were reported, suggesting that BLG is a promising material for spin qubits.

In addition to spin, the valley pseudospin is another degree of freedom in graphene and other van der Waals materials, arising from their two-dimensional honeycomb lattice structure. While in the two-dimensional transition-metal dichalcogenides, the strong spin-orbit coupling locks the spin and valley degrees of freedom together, leading to interesting combinations of spin and valley qubits [21–23], the weak spin-orbit coupling in graphene ensures that the spin and valley degrees of freedom are nearly independent. Specifically, BLG has two independent energy valleys located at the $\boldsymbol{K}$ and $\boldsymbol{K}'$ points of the hexagonal Brillouin zone. With broken spatial inversion symmetry, the two inequivalent valleys in gapped BLG experience opposite Berry curvatures and associated orbital magnetic moments [24–26]. This leads to a valley splitting which grows linearly in the applied out-of-plane magnetic field, and which can be viewed as a valley Zeeman splitting similar to the spin Zeeman splitting. The valley Zeeman effect has already been demonstrated recently by single-carrier measurements in BLG QDs [27]. This effect provides a promising path towards controlling the valley degree of freedom and to further establish valley-based electronics (valleytronics) [28,29] as well as valley-based qubits in graphene QDs [30,31]. To assess the potential of valley bits and qubits, the valley relaxation time of single-electron states in a BLG QD is a crucial parameter since it limits the lifetime of both the encoded classical and quantum information. Recently, Banszerus *et al.* measured valley relaxation times as large as several microseconds using pulsed-gate spectroscopy [32]. In the out-of-plane magnetic-field dependence of valley relaxation time, a monotonic decay at higher fields and a peak at smaller fields was observed. To explain the experiment, theoretical work on valley relaxation in BLG QDs is required.

In this paper, we investigate both the bound-state energy levels and the valley relaxation time of a single-electron BLG QD as a function of the out-of-plane magnetic fields $B_\perp$ (see Fig. 1). We employ an exact diagonalization method to obtain the energy levels and the eigenstates. At zero magnetic field, the lowest four energy levels form two Kramers pairs separated by an intrinsic spin-orbit gap. At finite magnetic fields, the energy levels become linearly dependent on $B_\perp$ due to both spin and valley Zeeman effects. At the value of $B_\perp$ where the intrinsic spin-orbit gap and valley Zeeman energy splitting coincide, intervalley scattering causes an anticrossing between the two different valley states. Based on the single-electron spectrum of the BLG QD, we then calculate the valley relaxation time using Fermi's golden rule. The valley relaxation channels are enabled by the intervalley coupling together with (i) $1/f$ charge noise and (ii) electron-phonon coupling via the deformation potential and the bond-length change. We find a peak at lower fields and a monotonic decay at higher fields. The low-field peak arises from the competition between the contributions of $1/f$ charge noise and bond-length change electron-phonon coupling. The monotonic decay at higher fields is due to the dominant contribution of the deformation potential. Moreover, we find that the interlayer hopping γ_3 opens a valley relaxation channel for electric charge noise when the quantum dot has rotational symmetry. Upon detailed comparison with the experiment [32], we find a good agreement between experiment and theory at higher magnetic fields.

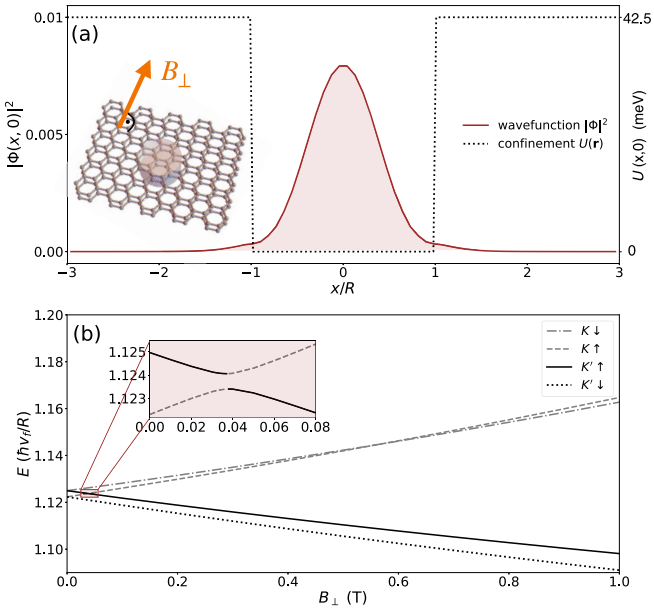

FIG. 1. (a) Calculated electronic probability density $|\phi(x)|^2$ (brown solid curve) of the lowest-energy level at $B_\perp = 0.2$ T as a function of position x for fixed $y = 0$. An electrostatic step potential (black dotted curve) defines a QD of radius R. Inset: Schematic picture of a BLG QD. (b) Bound-state energy levels as a function of perpendicular magnetic field $B_\perp$ in a BLG QD. The energy splitting between different valleys is dominated by the valley Zeeman effect with the valley g-factor g_v. From our calculation (shown in this plot) we extract $g_v = 31$. The anticrossing between the bound states $\boldsymbol{K}\uparrow$ and $\boldsymbol{K}'\uparrow$ is enlarged in the inset. For this calculation, we have set $U_0 = 42.5$ meV, $V = 25$ meV, $R = 25$ nm, $\Delta_i = 43$ μeV, and $\Delta_{KK'} = 10$ μeV. Energies are plotted in units of $\hbar v_f/R$ where v_f denotes the Fermi velocity (see Table I).

The remainder of this paper is organized as follows. In Sec. II we describe our model and the methods used for the calculation of the valley relaxation time. In Sec. III we describe the relevant mechanisms that contribute to valley relaxation, and in Sec. IV we show the resulting valley relaxation times obtained from the numerical evaluation of our model. Finally, we conclude our work in Sec. V.

II. MODEL AND METHOD

We consider Bernal (AB) stacked BLG in the presence of a homogeneous out-of-plane magnetic field $B_\perp$ and an electrostatic confinement potential $U(\mathbf{r})$ with $\mathbf{r} = (x, y)$. The total single-particle Hamiltonian can be written as

$$H_{\mathrm{QD}} = H^\tau(\mathbf{k}) + U(\mathbf{r}) + H_{\mathrm{SO}} + H_{\mathrm{Z}} + H_{KK'}, \tag{1}$$

where $H^\tau(\mathbf{k})$ is an effective 4×4 Hamiltonian describing the spinless π-band structure of BLG near the $\boldsymbol{K}$ and $\boldsymbol{K}'$ valleys [2,33],

$$H^\tau(\mathbf{k}) = \begin{pmatrix} V & \gamma_0 p & \gamma_4 p^* & \gamma_1 \\ \gamma_0 p^* & V & \gamma_3 p & \gamma_4 p^* \\ \gamma_4 p & \gamma_3 p^* & -V & \gamma_0 p \\ \gamma_1 & \gamma_4 p & \gamma_0 p^* & -V \end{pmatrix}, \tag{2}$$

TABLE I. Parameters used in the calculation: $\gamma_{0,1,3,4}$, g_s, and a are introduced in Eq. (1), $v_{\mathrm{TA,LA}}$ and ρ are used in Eq. (4), and v_f appears in Fig. 1.

γ_0	2.6 eV	γ_1	0.339 eV
γ_3	0.28 eV	γ_4	−0.14 eV
g_s	2	a	2.46 Å
v_{TA}	1.22×10^4 m/s	v_{LA}	1.95×10^4 m/s
v_f	8×10^5 m/s	ρ	1.52×10^{-7} g/cm^{-2}

in the on-site orbital Bloch basis $\Psi_{A_1}(\mathbf{k})$, $\Psi_{B_1}(\mathbf{k})$, $\Psi_{A_2}(\mathbf{k})$, and $\Psi_{B_2}(\mathbf{k})$, where A_1 and B_1 refer to the A and B sublattices in the lower layer, A_2 and B_2 denote the A and B sublattices in the upper layer, and $\mathbf{k} = (k_x, k_y)$ represents the two-dimensional wave vector measured from the $\boldsymbol{K}$ ($\tau = 1$) or $\boldsymbol{K}'$ ($\tau = -1$) point. Here, $2V$ describes the potential difference between the two graphene layers, which is controlled by an out-of-plane electric field, and γ_0 and γ_1 represent the nearest-neighbor intralayer and interlayer hoppings whereas γ_3 and γ_4 are the indirect hopping parameters between the two layers. The momentum dependence is given by $p(\mathbf{k}) = -\sqrt{3}a(\tau k_x - ik_y - ixB_\perp e/2 - \tau y B_\perp e/2)/2$ which includes the orbital effect due to the out-of-plane magnetic field, with a being the lattice constant. The second term in Eq. (1) is the confinement potential, which for simplicity is chosen to be a finite circularly symmetric step potential,

$$U(\mathbf{r}) = \begin{cases} U_0, & r \geqslant R, \\ 0, & r < R, \end{cases} \tag{3}$$

where U_0 and R denote the potential depth and QD radius, respectively. The third term $H_{\mathrm{SO}} = \Delta_i \tau \sigma_z s_z + \Delta_R(\tau \sigma_x s_y - \sigma_y s_x)$ describes the spin-orbit coupling with strength Δ_i (Δ_R) for the intrinsic (Rashba) spin-orbit effects, and $\sigma_{x,y,z}$ ($s_{x,y,z}$) are the Pauli matrices for the sublattice (spin) degree of freedom. While the intrinsic spin-orbit coupling does not contribute to the intervalley mixing, it does have an effect on the spin and valley resolved QD energy levels. Note however that the contribution of the Rashba term is negligible and therefore we take Δ_R to be zero throughout this paper. The fourth term describes the spin Zeeman coupling as $H_Z = g_s \mu_B s_z B_\perp/2$ with g_s the spin g factor and μ_B the Bohr magneton. The last term $H_{KK'} = \Delta_{KK'}\tau_x/2$ represents the intervalley coupling possibly induced by disorder where $\Delta_{KK'}$ quantifies the intervalley coupling strength and τ_x denotes the Pauli x matrix for valley [27,34]. All the parameters are listed in Table I.

Note that in the absence of the Rashba term, the total Hamiltonian (1) can be divided into two independent spin blocks, i.e., spin up and spin down. Within each spin block, we first solve the Schrödinger equation of the Hamiltonian $H_0 = H^\tau(\mathbf{k}) + U(\mathbf{r})$ numerically by discretizing two-dimensional real space using a square lattice grid. To rid ourselves of the Fermi doubling problem arising from the lattice discretization, we include a Wilson mass term wk^2 in H_0 with w denoting the Wilson mass [35]. Then, we take into account the remaining terms in Eq. (1) in the eigenbasis of H_0 in both valleys. Finally, we can exactly diagonalize the total Hamiltonian and obtain single-particle eigenvalues and eigenfunctions which we plot in Fig. 1(b).

III. VALLEY RELAXATION MECHANISMS

With the eigenvalues and eigenstates at hand, we can now calculate the valley relaxation rate from the initial state $|i\rangle$ to the final state $|f\rangle$ using Fermi's golden rule. Here, we consider valley relaxation due to (i) the electron-phonon coupling via the deformation potential and the bond-length change mechanisms [36–38], and (ii) $1/f$ charge noise [39,40].

A. Relaxation induced by electron-phonon coupling

We consider two different electron-phonon interaction mechanisms, the deformation potential on the one hand and the bond-length change on the other. The deformation potential is induced by a phonon-induced area change in the unit cell, whereas the bond-length change is caused by a modified hopping matrix element. Since we are interested in the low-energy regime, only acoustic phonons near the Γ point are considered. Furthermore, out-of-plane phonon modes are irrelevant since we assume that the host BLG sheet is placed on a substrate. Therefore, we take into account in-plane longitudinal-acoustic (LA) and transverse-acoustic (TA) modes only. The intravalley electron-phonon coupling is described in the sublattice basis as [41]

$$H_{\mathrm{EPC}}^{\lambda\mathbf{q}} = \frac{q}{\sqrt{A\rho\Omega_{\mathbf{q},\lambda}}}\begin{pmatrix} g_1 a_1 & g_2 a_2^* \\ g_2 a_2 & g_1 a_1 \end{pmatrix}(e^{i\mathbf{q}\cdot\mathbf{r}} b_{\lambda\mathbf{q}}^\dagger - e^{-i\mathbf{q}\cdot\mathbf{r}} b_{\lambda\mathbf{q}}), \quad (4)$$

with A the area of the graphene sheet, ρ the mass density of BLG, g_1 (g_2) the coupling strength of the deformation potential (bond-length change), $a_1 = i$ and $a_2 = ie^{2i\phi_{\mathbf{q}}}$ for LA phonons, and $a_2 = e^{2i\phi_{\mathbf{q}}}$ and $a_1 = 0$ for TA phonons. The phonon energy is given by $\Omega_{\mathbf{q},\lambda} = v_\lambda q$ with v_λ the sound velocity for the phonon branch $\lambda = \mathrm{TA}, \mathrm{LA}$, while $b_{\lambda\mathbf{q}}^\dagger$ and $b_{\lambda\mathbf{q}}$ denote the creation and annihilation operators for branch λ phonons with wave vector $\mathbf{q}$. Considering the weak coupling between the two graphene layers, we can approximate the bilayer electron-phonon coupling as the combination of the single-layer electron-phonon couplings for each layer separately [33].

Using Fermi's golden rule, we can calculate the valley relaxation rate due to electron-phonon coupling from $|i\rangle$ with energy ϵ_i to $|f\rangle$ with energy ϵ_f away from the anticrossing shown in Fig. 1(b) as

$$\frac{1}{T_1} = 2\pi A \sum_\lambda \int \frac{d^2q}{(2\pi)^2} \left|\langle i|H_{\mathrm{EPC}}^{\lambda\mathbf{q}}|f\rangle\right|^2 \delta(\epsilon_f - \epsilon_i + \Omega_{\mathbf{q},\lambda}). \quad (5)$$

The relaxation process is only possible due to the presence of the intervalley coupling $H_{KK'}$ in H_{QD} which leads to a small intervalley mixing in the eigenstates $|i\rangle$ and $|f\rangle$ of H_{QD}. This so-called admixture mechanism is known from spin relaxation [42] and allows for valley relaxation via the valley-preserving electron-phonon coupling. Note that only the phonon emission process is taken into account here by assuming that the temperature is much lower than the valley splitting.

B. Relaxation induced by $1/f$ charge noise

Electric (charge) noise with its typical $1/f$ power spectral density often arises as a consequence of fluctuating two-level systems in the environment of the localized QD electron. More precisely, the electric charge noise spectra can be given by $S_{\mathrm{E}}(\omega) = S_0/\omega^\alpha$ where S_0 stands for the power spectral density at 1 Hz and the exponent α is device dependent and typically reported to be between 0.5 and 2 [43]. We can calculate the valley relaxation rate from $|i\rangle$ to $|f\rangle$ away from the anticrossing shown in Fig. 1(b) using

$$\frac{1}{T_1} = \frac{4\pi e^2}{\hbar^2} S_{\mathrm{E}}(\epsilon_i - \epsilon_f) \sum_j |\langle i|r_j|f\rangle|^2 \quad (6)$$

$$= \frac{4\pi e^2}{\hbar^2} S_{\mathrm{E}}(\epsilon_i - \epsilon_f) \frac{|\langle i|r_+|f\rangle|^2 + |\langle i|r_-|f\rangle|^2}{2}, \quad (7)$$

with $\mathbf{r} = (x, y)$ and $r_\pm = x \pm iy$ [39,40].

In the absence of γ_3 in (2), the Hamiltonian of each valley has rotational symmetry and hence commutes with the total angular-momentum operator $J_z = L_z + \tau\hbar(\sigma_z/2 - \eta_z/2)$. Here, L_z and η_z represent the orbital angular momentum operator and the Pauli z matrix for the layer degree of freedom, respectively. Thus, we have $J_z\Phi(\tau, m) = m\hbar\Phi(\tau, m)$ where $\Phi(\tau, m)$ is an eigenstate within each valley $\tau = \pm 1$. Due to the existence of the intervalley coupling $H_{KK'}$, the states $\Phi(\tau = 1, m_1)$ in the K valley can be coupled to the states $\Phi(\tau = -1, m_2)$ in the K' valley with coupling matrix element $M_{KK'}^{m_1 m_2} = \Delta_{KK'}\Phi^\dagger(\tau = 1, m_1)\Phi(\tau = -1, m_2)/2$. It is easy to demonstrate that $M_{KK'}^{m_1 m_2}$ is nonzero only when $m_1 = m_2$. This means that only the states with the same angular momentum in two valleys are coupled. Further, by referring to Eq. (7), the valley relaxation due to $1/f$ noise is absent unless the angular momentum between the initial and final states differs by ± 1. This can be used as a selection rule for valley relaxation due to $1/f$ noise in the presence of rotational symmetry. This selection rule can be generalized to other types of electric charge noise.

IV. NUMERICAL RESULTS

In Fig. 1(a), we show a schematic picture of a BLG QD defined by an electrostatic step potential. The probability density associated with the lowest-energy level at $B_\perp = 0.2$ T is plotted as a function of the coordinate x for fixed $y = 0$. This indicates that the wave function is localized within the QD. We then calculate the lowest four bound-state energy levels as a function of out-of-plane magnetic field, shown in Fig. 1(b) with labels $|K\uparrow\rangle$, $|K\downarrow\rangle$, $|K'\uparrow\rangle$, and $|K'\downarrow\rangle$. At zero magnetic field, we find two Kramers pairs ($|K\uparrow\rangle$, $|K'\downarrow\rangle$) and ($|K\downarrow\rangle$, $|K'\uparrow\rangle$), separated by the intrinsic spin-orbit gap of around 70 μ eV. At finite magnetic fields, all of these energy levels show a linear dependence with slopes $\frac{1}{2}(\pm g_s \pm g_v)\mu_B$ according to the spin and valley Zeeman effects. Here, we find $g_v = 31.0$ as the valley g factor. In addition, we find an anticrossing between the states $|K\uparrow\rangle$ and $|K'\uparrow\rangle$, which is enlarged in the inset of Fig. 1(b). This anticrossing results from the intervalley coupling $H_{KK'}$.

A. Valley relaxation: Theoretical calculation

As mentioned previously, in the absence of the Rashba spin-orbit term, our system is divided into two independent sectors, one with spin up and another with spin down. Then, the valley relaxation time can be calculated within each spin sector. Since the valley relaxation times of spin up and spin

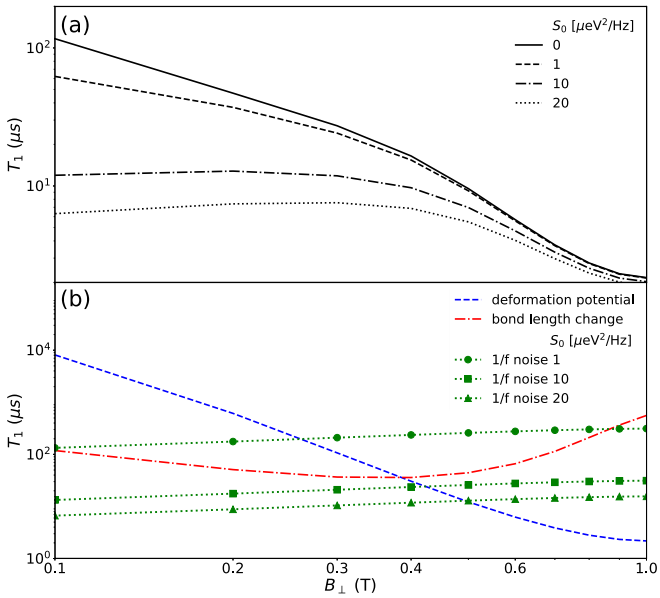

FIG. 2. (a) Total valley relaxation time T_1 as a function of perpendicular field $B_\perp$ on a double-logarithmic scale, for different noise strengths $S_0 = 0, 1, 10, 20$ μeV^2/Hz ($1/f$ noise). (b) Valley relaxation time due to deformation potential (blue dashed curve), bond-length change (red dotted-dashed curve), and $1/f$ charge noise (green dotted curves). For the $1/f$ charge noise, $S_0 = 1, 10, 20$ μeV^2/Hz are represented by dots, squares, and triangles, respectively. In the calculation, we have used $U_0 = 42.5$ meV, $V = 25$ meV, $R = 25$ nm, $\Delta_i = 43$ μeV, $\Delta_{KK'} = 10$ μeV, $g_1 = 50$ eV, $g_2 = 2.8$ eV, and $\alpha = 0.5$.

down are very close to each other, we focus on the spin-down sector in the present work.

In Fig. 2(a), the total resulting valley relaxation time is plotted as a function of the perpendicular magnetic field $B_\perp$ for different values of S_0 characterizing the strength of the $1/f$ noise. In the absence of $1/f$ charge noise, the valley relaxation time shows a monotonic decrease with increasing magnetic field. With finite $1/f$ charge noise, the valley relaxation time becomes much shorter at lower fields, indicating that $1/f$ charge noise plays a more important role at lower fields. In addition, a peak is predicted at lower fields for sufficiently strong $1/f$ noise (large S_0). To understand these behaviors, we show the contributions of deformation potential, bond-length change, and $1/f$ charge noise separately in Fig. 2(b). In the absence of $1/f$ charge noise, the valley relaxation is dominated by the bond-length change (deformation potential) at lower (higher) fields. Both the valley relaxation time due to the bond-length change at lower fields and the deformation potential at higher fields decrease with increasing magnetic field, arising from the increase of the valley splitting, i.e., the energy splitting between initial and final states. This gives rise to a monotonic decrease of valley relaxation time. When $1/f$ charge noise comes into play, the valley relaxation at higher fields is still dominated by the deformation potential. However, at lower fields, there exists a competition between the $1/f$ noise and bond-length change when the noise spectral density is strong. This competition leads to a peak in the magnetic-field dependence.

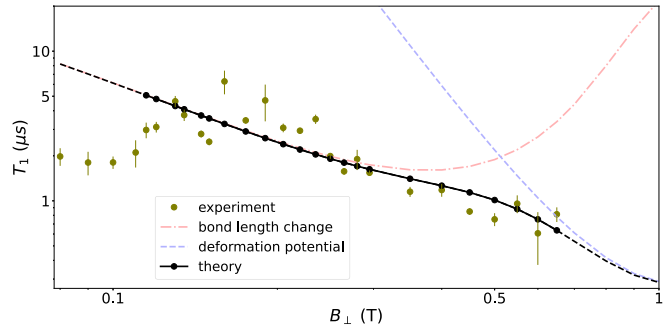

FIG. 3. Log-log plot of the valley relaxation time T_1 as a function of perpendicular magnetic field $B_\perp$. The olive dots stand for the experimental data from Ref. [32], while the black curve with dots represents the theoretical result obtained by fitting to the experimental data using least-squares method with fitting parameters $g_1 = 50$ eV, $g_2 = 5.4$ eV, $\Delta_{KK'} = 50$ μeV, $R = 25$ nm, $U_0 = 39.6$ meV, and $\Delta_i = 35$ μeV. The blue dashed curve (red dotted-dashed curve) denotes the valley relaxation time due to deformation potential (bond-length change).

In addition, we also investigate the valley relaxation with different exponents α in the $1/f$ charge noise power spectral density. We find that with increasing α, the valley relaxation time exhibits an overall increase. In particular, the increase at lower fields is dramatic, suggesting the importance of $1/f$ charge noise at lower fields. Similar to the situation of different noise spectral densities mentioned above, a peak is also observed in the magnetic-field dependence for small α, attributed to the competition between $1/f$ charge noise and the bond-length change mechanism.

B. Comparison with experiment

Very recently, Banszerus *et al.* [32] reported experimental single-particle valley relaxation times in a BLG QD as a function of perpendicular magnetic field, shown in Fig. 3 as olive dots. At higher fields, a monotonic decay is observed. To explain this behavior, we take into account the contribution of deformation potential and bond-length change, while $1/f$ charge noise is not included due to its negligible contribution at higher fields. We perform a least-squares fit of the electron-phonon coupling strengths g_1 and g_2 to the measurement data, taking into account the experimental error bars. The result of our numerical fit is shown as the black curve with dots, which agrees with the experimental data both qualitatively and quantitatively. At lower fields, a peak is observed in the experimental data. Our theory suggests that the origin of this peak lies in a competition between electric noise and phonons. However, similar peaks may also arise from a competition between different electron-phonon coupling mechanisms or from a valley crossing. Further research can shed more light on the origin of the nonmonotonic behavior of $T_1(B_\perp)$.

V. CONCLUSIONS AND DISCUSSION

We have studied the electronic valley relaxation time T_1 in a BLG QD with magnetic field $B_\perp$ perpendicular to the graphene plane. The valley relaxation is induced

by the intervalley coupling together with $1/f$ charge noise and electron-phonon scattering via deformation potential and bond-length change. In the magnetic-field dependence of valley relaxation time, a peak at lower fields and a monotonic decay at higher fields are predicted, which agree with a recent experiment [32]. The origin of the peak at lower fields is explained as arising from the competition between the contributions of $1/f$ noise and phonon emission via bond-length change. The monotonic decay for large $B_\perp$ is due to the contribution of both the deformation potential and bond-length change at higher fields. In addition, we show that while the contribution of $1/f$ charge noise to valley relaxation is more important at lower fields due to smaller noise frequency, at higher fields the deformation potential dominates the valley relaxation process.

The valley relaxation has also been studied in a BLG device containing gate-defined double QDs where the valley relaxation time between the valley triplet and singlet states was reported to be remarkably long [44]. This experiment requires future research to understand the singlet-triplet valley relaxation mechanisms.

ACKNOWLEDGMENT

We would like to acknowledge P. M. Mutter for fruitful discussions.

[1] E. McCann and V. I. Fal'ko, Phys. Rev. Lett. **96**, 086805 (2006).
[2] S. Konschuh, M. Gmitra, D. Kochan, and J. Fabian, Phys. Rev. B **85**, 115423 (2012).
[3] E. McCann and M. Koshino, Rep. Prog. Phys. **76**, 056503 (2013).
[4] H. Min, B. Sahu, S. K. Banerjee, and A. H. MacDonald, Phys. Rev. B **75**, 155115 (2007).
[5] E. V. Castro, K. S. Novoselov, S. V. Morozov, N. M. R. Peres, J. M. B. Lopes dos Santos, J. Nilsson, F. Guinea, A. K. Geim, and A. H. Castro Neto, Phys. Rev. Lett. **99**, 216802 (2007).
[6] Y. Zhang, T.-T. Tang, C. Girit, Z. Hao, M. C. Martin, A. Zettl, M. F. Crommie, Y. R. Shen, and F. Wang, Nature (London) **459**, 820 (2009).
[7] J. Nilsson, A. H. Castro Neto, F. Guinea, and N. M. R. Peres, Phys. Rev. B **78**, 045405 (2008).
[8] B. Trauzettel, D. V. Bulaev, D. Loss, and G. Burkard, Nat. Phys. **3**, 192 (2007).
[9] C. L. Kane and E. J. Mele, Phys. Rev. Lett. **95**, 226801 (2005).
[10] D. Huertas-Hernando, F. Guinea, and A. Brataas, Phys. Rev. B **74**, 155426 (2006).
[11] H. Min, J. E. Hill, N. A. Sinitsyn, B. R. Sahu, L. Kleinman, and A. H. MacDonald, Phys. Rev. B **74**, 165310 (2006).
[12] Y. Yao, F. Ye, X.-L. Qi, S.-C. Zhang, and Z. Fang, Phys. Rev. B **75**, 041401(R) (2007).
[13] J. C. Boettger and S. B. Trickey, Phys. Rev. B **75**, 121402(R) (2007).
[14] J. Fischer, B. Trauzettel, and D. Loss, Phys. Rev. B **80**, 155401 (2009).
[15] M. Gmitra, S. Konschuh, C. Ertler, C. Ambrosch-Draxl, and J. Fabian, Phys. Rev. B **80**, 235431 (2009).
[16] D. Huertas-Hernando, F. Guinea, and A. Brataas, Phys. Rev. Lett. **103**, 146801 (2009).
[17] S. Abdelouahed, A. Ernst, J. Henk, I. V. Maznichenko, and I. Mertig, Phys. Rev. B **82**, 125424 (2010).
[18] S. Konschuh, M. Gmitra, and J. Fabian, Phys. Rev. B **82**, 245412 (2010).
[19] L. Banszerus, K. Hecker, S. Möller, E. Icking, K. Watanabe, T. Taniguchi, C. Volk, and C. Stampfer, Nat. Commun. **13**, 3637 (2022).
[20] L. M. Gächter, R. Garreis, J. D. Gerber, M. J. Ruckriegel, C. Tong, B. Kratochwil, F. K. de Vries, A. Kurzmann, K. Watanabe, T. Taniguchi, T. Ihn, K. Ensslin, and W. W. Huang, PRX Quantum **3**, 020343 (2022).
[21] M. Brooks and G. Burkard, Phys. Rev. B **101**, 035204 (2020).
[22] R. Krishnan, S. Biswas, Y.-L. Hsueh, H. Ma, R. Rahman, and B. Weber, Nano Lett. **23**, 6171 (2023).
[23] T. Aliyar, H. Ma, R. Krishnan, G. Singh, B. Q. Chong, Y. Wang, I. Verzhbitskiy, C. P. Yu Wong, K. E. Johnson Goh, Z. X. Shen, T. S. Koh, R. Rahman, and B. Weber, Nano Lett. **24**, 2142 (2024).
[24] A. Knothe and V. Fal'ko, Phys. Rev. B **98**, 155435 (2018).
[25] M. Eich, R. Pisoni, A. Pally, H. Overweg, A. Kurzmann, Y. Lee, P. Rickhaus, K. Watanabe, T. Taniguchi, K. Ensslin *et al.*, Nano Lett. **18**, 5042 (2018).
[26] L. Banszerus, A. Rothstein, T. Fabian, S. Möller, E. Icking, S. Trellenkamp, F. Lentz, D. Neumaier, K. Watanabe, T. Taniguchi *et al.*, Nano Lett. **20**, 7709 (2020).
[27] L. Banszerus, S. Möller, C. Steiner, E. Icking, S. Trellenkamp, F. Lentz, K. Watanabe, T. Taniguchi, C. Volk, and C. Stampfer, Nat. Commun. **12**, 5250 (2021).
[28] A. Rycerz, J. Tworzydło, and C. Beenakker, Nat. Phys. **3**, 172 (2007).
[29] J. R. Schaibley, H. Yu, G. Clark, P. Rivera, J. S. Ross, K. L. Seyler, W. Yao, and X. Xu, Nat. Rev. Mater. **1**, 16055 (2016).
[30] N. Rohling and G. Burkard, New J. Phys. **14**, 083008 (2012).
[31] N. Rohling, M. Russ, and G. Burkard, Phys. Rev. Lett. **113**, 176801 (2014).
[32] L. Banszerus, K. Hecker, L. Wang, S. Möller, K. Watanabe, T. Taniguchi, G. Burkard, C. Volk, and C. Stampfer, arXiv:2402.16691.
[33] L. Wang and M. W. Wu, Phys. Rev. B **87**, 205416 (2013).
[34] J. Klinovaja, G. J. Ferreira, and D. Loss, Phys. Rev. B **86**, 235416 (2012).
[35] B. Messias de Resende, F. C. de Lima, R. H. Miwa, E. Vernek, and G. J. Ferreira, Phys. Rev. B **96**, 161113(R) (2017).
[36] P. R. Struck and G. Burkard, Phys. Rev. B **82**, 125401 (2010).
[37] M. Droth and G. Burkard, Phys. Rev. B **84**, 155404 (2011).
[38] M. Droth and G. Burkard, Phys. Rev. B **87**, 205432 (2013).
[39] A. Hosseinkhani and G. Burkard, Phys. Rev. B **104**, 085309 (2021).

[40] A. Hosseinkhani and G. Burkard, Phys. Rev. B **106**, 075415 (2022).
[41] T. Ando, J. Phys. Soc. Jpn. **74**, 777 (2005).
[42] A. V. Khaetskii and Y. V. Nazarov, Phys. Rev. B **64**, 125316 (2001).
[43] L. Kranz, S. K. Gorman, B. Thorgrimsson, Y. He, D. Keith, J. G. Keizer, and M. Y. Simmons, Adv. Mater. **32**, 2003361 (2020).
[44] R. Garreis, C. Tong, J. Terle, M. J. Ruckriegel, J. D. Gerber, L. M. Gächter, K. Watanabe, T. Taniguchi, T. Ihn, K. Ensslin, and W. W. Huang, Nat. Phys. **20**, 428 (2024).